Temporal modulation instabilities of counterpropagating waves in a finite dispersive Kerr medium. I. Theoretical model and analysis

M. Yu and C. J. McKinstrie

Department of Mechanical Engineering and Laboratory for Laser Energetics, University of Rochester, Rochester, New York 14627

Govind P. Agrawal

The Institute of Optics, University of Rochester, Rochester, New York 14627

This paper presents a comprehensive analytical study of temporal modulation instabilities in a finite, nonlinear, dispersive medium in which two counterpropagating pump beams interact through a Kerr-type nonlinearity. The analysis includes self- and cross-phase modulations, group-velocity dispersion, four-wave mixing, and reflections occurring at the two facets of the dispersive Kerr medium. The use of a new method based on a small-parameter analysis has resulted in a physically transparent model in terms of a doubly resonant optical parametric oscillator that allows characterization of the complicated nonlinear system in a familiar language. The effects of boundary reflections are shown to be very important. In the low-frequency limit, in which dispersive effects are negligible, our results reduce to those obtained previously. At high frequencies, dispersive effects lead to new instabilities both in the normal- and anomalous-dispersion regions of the dispersive Kerr medium. The anomalous-dispersion case is discussed in detail after including weak boundary reflections. The growth rate and the threshold for the absolute instability are obtained in an analytical form for arbitrary pump–power ratios. Our analytic results are in agreement with previous numerical work done by neglecting boundary reflections and assuming equal powers for the counterpropagating pump beams. © 1998 Optical Society of America [S0740-3224(98)04202-7]

OCIS codes: 190.0190, 190.3270, 120.2230, 270.3100.

1. INTRODUCTION

The nonlinear interaction between counterpropagating waves in a finite Kerr medium has been studied extensively[1–6] because of its relevance to many practical optical devices such as optical gyroscopes, lasers, fiber interferometers, and optically bistable switches. Such interaction exhibits rich nonlinear dynamics ranging from bistability to optical chaos, since the Kerr nonlinearity tends to destabilize the steady-state propagation of the counterpropagating pump waves.

Instabilities are classified into two categories, known as convective and absolute. Even for a Kerr medium without group-velocity dispersion (GVD), an absolute temporal instability of the counterpropagating pump waves can occur in the presence of boundary reflections, which effectively form a Fabry–Perot (FP) cavity.[1,2] This instability has been shown to be an FP-cavity version of the Ikeda instability[7] (first found in a ring cavity for a unidirectional pump beam), and can be explained in terms of a four-wave-mixing (FWM) process. The effects of diffraction and dispersion were included later[3–5] and were found to affect the instability substantially.

Dispersive effects come into play at high temporal frequencies and must be included if the Kerr medium is also dispersive. Considerable attention has been paid to studying the effects of GVD on optical instabilities occurring in Kerr media. It is well known that the spectral sidebands of a unidirectional pump wave can be amplified by the convective modulation instability (MI) owing to the combined effect of FWM and anomalous GVD.[8] This MI can become an absolute instability inside a ring cavity because of the feedback loop.[9–11] In fact, MI lasers have been proposed and demonstrated for the ring-cavity configuration.[12,13] Like the temporal GVD effects, spatial diffractive effects have also been considered for the ring cavity.[14,15]

Compared with the case of a unidirectional ring cavity, the inclusion of GVD effects in a finite medium with counterpropagating pump waves is much more difficult, mainly because the nonlinear interaction involves two pairs of sidebands (one pair for each pump wave). Such interaction is induced by both self-phase modulation and cross-phase modulation. Previous work has found that even when the boundary reflections are neglected, the counterpropagating pump waves in a finite medium can become *absolutely* unstable.[4,5] However, the treatment was quite involved mathematically and did not provide physical insight, since an eigenvalue problem in a four-dimensional vector space has to be solved numerically. Consequently, the studies were limited to the special case

of counterpropagating pump beams with nearly equal power levels. It is thus desirable to establish an analytic model that can give a clear physical picture and, at the same time, provide an analytical result for the more general case of unequal pump powers. Moreover, it is not clear how the instability would be affected by the weak boundary reflections that always exist in practice. The nonlinear dynamics can become quite intriguing in such a case since the boundary reflections provide additional coupling between the two pairs of sidebands.

In this paper, we study the combined effects of GVD, cross- and self-phase modulation, and boundary reflections on the stability of counterpropagating pump waves in a dispersive Kerr medium. Although the case of silica fibers is used as an example, the results are applicable to any dispersive Kerr medium. A simple physical model is proposed based on a small-parameter perturbation analysis. It allows us to obtain the analytical expressions for the threshold and the growth rate of the absolute instability. Our results agree with the previous work when the boundary reflections are zero and the two pump powers are equal.

The paper is organized as follows. In Section 2, we carry out a linear-stability analysis of the coupled nonlinear Schrödinger equations, which describe the propagation of counterpropagating pump waves in a dispersive Kerr medium, and obtain a general solution governing the evolution of four sidebands. The theoretical model is completed in Section 3, where boundary reflections are incorporated and the appropriate parameter regime is identified. The results are used in Section 4 to discuss absolute instability in the case of weak reflections from the boundary of the nonlinear medium. The main results are summarized in Section 5.

2. GENERAL SOLUTION

The nonlinear system under investigation is illustrated in Fig. 1. Two counterpropagating pump waves interact in a dispersive Kerr medium of length l. The diffractive effects are ignored for simplicity, thereby reducing the problem to only one spatial dimension. The analysis is directly applicable to a single-mode waveguide such as an optical fiber. It can also be used for bulk nonlinear media provided the beam size is large enough that the diffraction length is much longer than the dispersion and nonlinear lengths introduced later. When this condition is not satisfied, new diffraction-induced transverse instabilities can occur[3] that are excluded from our analysis.
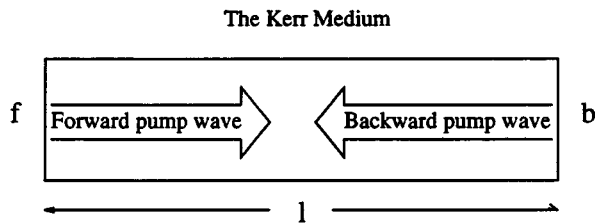
The Kerr Medium

Fig. 1. Schematic illustration of a finite dispersive Kerr medium of length l in which two counterpropagating pump waves interact nonlinearly with each other. The front and back surface are labeled f and b, respectively.

We also assume that the pump polarization is not affected during propagation, thereby excluding polarization instabilities. With these simplifications and making the scalar-wave and the slowly-varying-envelope approximations, the nonlinear interaction of two counterpropagating optical waves in a dispersive Kerr medium is described by the following two coupled nonlinear Schrödinger equations[8]:

$$i\,\frac{\partial A_1}{\partial z} + i\beta_1\,\frac{\partial A_1}{\partial t} = \frac{1}{2}\,\beta_2\,\frac{\partial^2 A_1}{\partial t^2} - \gamma(|A_1|^2 + 2|A_2|^2)A_1,$$
(1)

$$-i\,\frac{\partial A_2}{\partial z} + i\beta_1\,\frac{\partial A_2}{\partial t} = \frac{1}{2}\,\beta_2\,\frac{\partial^2 A_2}{\partial t^2} - \gamma(|A_2|^2 + 2|A_1|^2)A_2,$$
(2)

where β_1^{-1}, β_2, and γ are the group velocity, the GVD coefficient, and the nonlinear parameter, respectively. The parameter γ is related to the Kerr coefficient n_2 as $\gamma = 2\pi n_2/(\lambda a_{\text{eff}})$, where λ is the optical wavelength and a_{eff} is the effective mode cross section. $A_1(t, z)$ and $A_2(t, z)$ are the complex envelopes of the forward and backward-propagating waves, respectively, and are related to the corresponding electric fields as

$$E_1(t, z) = \text{Re}\{A_1(t, z)\exp(ik_0 z - i\omega_0 t)\},$$
(3)

$$E_2(t, z) = \text{Re}\{A_2(t, z)\exp[ik_0(l - z) - i\omega_0 t]\},$$
(4)

where Re stands for the real part, ω_0 is the frequency of the pump beams, $k_0 = \omega_0/c$ is the corresponding propagation constant, and l is the length of the Kerr medium. The constant phase factor $\exp(ik_0 l)$ in Eq. (4) has been sorted out for later convenience, and the fields have been normalized such that $|A_1|^2$ and $|A_2|^2$ represent the powers of the two pump beams.

The counterpropagating cw pump fields in the medium correspond to the steady-state solutions of Eqs. (1) and (2), given by

$$A_{1s}(t, z) = A_{10}\exp[i\gamma(|A_{10}|^2 + 2|A_{20}|^2)z],$$
(5)

$$A_{2s}(t, z) = A_{20}\exp[i\gamma(|A_{20}|^2 + 2|A_{10}|^2)(l - z)],$$
(6)

where the constants $A_{10} = |A_{10}|\exp(i\phi_{10})$ and $A_{20} = |A_{20}|\exp(i\phi_{20})$ contain both the amplitude and phase information for the two counterpropagating waves in the medium. However, only their phase difference, $\phi_{20} - \phi_{10}$, is of physical significance because we can always assume, without loss of generality, that one of the phases is zero.

A. Linear-Stability Analysis
The stability of the steady-state solution is studied by performing a standard linear-stability analysis. For this purpose, we perturb the steady state slightly and write the respective perturbations for the two pump waves as

$$\delta A_1(t, z) = \overline{\delta A}_1(t, z) \exp[i\gamma(|A_{10}|^2 + 2|A_{20}|^2)z], \quad (7)$$

$$\delta A_2(t, z) = \overline{\delta A}_2(t, z) \exp[i\gamma(|A_{20}|^2 + 2|A_{10}|^2)(l - z)]. \quad (8)$$

By inserting $A_1 = A_{1s} + \delta A_1$ and $A_{2s} = A_{2s} + \delta A_2$ into Eqs. (1) and (2), the linearized equations for $\overline{\delta A}_1(t, z)$ and $\overline{\delta A}_2(t, z)$, written in the frequency domain, take the form

$$(i\partial/\partial z + \beta_1\omega + \beta_2\omega^2/2 + \gamma|A_{10}|^2)\delta A_1(\omega, z)$$
$$+ \gamma[A_{10}^2\delta A_1^*(-\omega, z) + 2A_{10}A_{20}^*\delta A_2(\omega, z)$$
$$+ 2A_{10}A_{20}\delta A_2^*(-\omega, z)] = 0, \quad (9)$$

$$(i\partial/\partial z - \beta_1\omega + \beta_2\omega^2/2 + \gamma|A_{10}|^2)\delta A_1^*(-\omega, z)$$
$$+ \gamma[A_{10}^{*2}\delta A_1(\omega, z) + 2A_{10}^*A_{20}\delta A_2^*(-\omega, z)$$
$$+ 2A_{10}^*A_{20}^*\delta A_2(\omega, z)] = 0, \quad (10)$$

$$(-i\partial/\partial z + \beta_1\omega + \beta_2\omega^2/2 + \gamma|A_{20}|^2)\delta A_2(\omega, z)$$
$$+ \gamma[A_{20}^2\delta A_2^*(-\omega, z) + 2A_{20}A_{10}^*\delta A_1(\omega, z)$$
$$+ 2A_{20}A_{10}\delta A_1^*(-\omega, z)] = 0, \quad (11)$$

$$(-i\partial/\partial z - \beta_1\omega + \beta_2\omega^2/2 + \gamma|A_{20}|^2)\delta A_2^*(-\omega, z)$$
$$+ \gamma[A_{20}^{*2}\delta A_2(\omega, z) + 2A_{20}^*A_{10}\delta A_1^*(-\omega, z)$$
$$+ 2A_{20}^*A_{10}^*\delta A_1(\omega, z)] = 0, \quad (12)$$

where $\delta A_1(\omega, z)$ and $\delta A_2(\omega, z)$ are the Fourier transforms of $\overline{\delta A}_1(t, z)$ and $\overline{\delta A}_2(t, z)$, respectively.

The standard Fourier-transform technique used to solve a set of coupled linear equations leads to the following general solution of Eqs. (9)–(12):

$$\begin{bmatrix} \delta A_1(\omega, z) \\ \delta A_1^*(-\omega, z) \\ \delta A_2(\omega, z) \\ \delta A_2^*(-\omega, z) \end{bmatrix} = \exp(ik_{1+}) \begin{bmatrix} 1 \\ r_{1+} \\ e_{1++} \\ e_{1+-} \end{bmatrix} c_1$$

$$+ \exp(ik_{1-}z) \begin{bmatrix} r_{1-} \\ 1 \\ e_{1-+} \\ e_{1--} \end{bmatrix} c_2$$

$$+ \exp[ik_{2+}(l - z)] \begin{bmatrix} e_{2++} \\ e_{2+-} \\ 1 \\ r_{2+} \end{bmatrix} c_3$$

$$+ \exp[ik_{2-}(l - z)] \begin{bmatrix} e_{2-+} \\ e_{2--} \\ r_{2-} \\ 1 \end{bmatrix} c_4, \quad (13)$$

where the arbitrary constants c_1, c_2, c_3, and c_4 represent the magnitudes of four independent eigenmodes of the solution, while the rest of the coefficients are functions of the modulation frequency ω. The quantities $k_{1\pm}$

and $k_{2\pm}$ represent the dispersion relations for the corresponding eigenmodes, and the coupling coefficients r_{ij} and e_{ijk} with $i = 1, 2$ and $j, k = +$ or $-$ govern relative amplitudes of the four sidebands [$\delta A_1(\omega, z)$, $\delta A_1^*(-\omega, z)$, $\delta A_2(\omega, z)$, and $\delta A_2^*(-\omega, z)$] for each eigenmode.

B. Small-Parameter Analysis

It is generally difficult to obtain the exact analytical expression for the dispersion relations and other coefficients in Eq. (13). For this reason, numerical studies have been performed in the past.[4,5] However, we show here that approximate analytical expressions can be obtained with sufficiently high precision by using a small-parameter analysis.

Before writing down the approximate analytical expressions, we introduce several characteristic lengths and frequencies. The walk-off length and the GVD length at a given modulation frequency ω are defined as $l_W = (\beta_1\omega)^{-1}$ and $l_D = (\beta_2\omega^2)^{-1}$. Note that the walk-off length for two counterpropagating waves is simply the spatial scale of envelope variations for the fields. Without loss of generality, we assume the power ratio $S \equiv |A_{20}|^2/|A_{10}|^2 \leq 1$ (i.e., the power of the backward-pump wave is equal to or less than the forward one). The nonlinear length at a given power of the forward-pump wave, $P = |A_{10}|^2$, is defined as $l_N = (\gamma|A_{10}|^2)^{-1}$. We further define $\omega_W = \gamma P/\beta_1$ and $\omega_D = (\gamma P/\beta_2)^{1/2}$ to represent the required modulation frequencies at which the walk-off length and the dispersion length are equal to the nonlinear length, respectively. For modulation frequencies below ω_W and ω_D, the effects of walk-off and GVD, respectively, are not important.

The ratio $\epsilon = \omega_W/\omega_D = (|\beta_2|\gamma P/\beta_1^2)^{1/2}$ is a small quantity if the power P and the GVD coefficient are not too large. Even for materials with a relatively large GVD coefficient and at relatively high powers, this ratio is still quite small, since in practice, the GVD effect is simply negligible when the walk-off length is comparable to the nonlinear length. In this paper, the dispersive nonlinear effects are of main concern, thus the normalized modulation frequency $\Omega = \omega/\omega_D$ and normalized length $L = l/l_N$ are often used. This means that the GVD effect is negligible when $\Omega \ll 1$, and the Kerr medium can be treated as dispersionless ($\beta_2 = 0$). Another ratio, $\epsilon_\Omega = l_W/l_D = \Omega\epsilon$, represents the relative importance of GVD over the walk-off at a given modulation frequency. This is also a small quantity since $\Omega \ll 1/\epsilon$ is usually satisfied.

Using silica fiber as an illustrative example,[8] we assume a forward-pump power of $P = 1$ kW, a nonlinear coefficient of $\gamma = 10$ W^{-1} km^{-1}, a group velocity of $1/\beta_1 = 0.2$ mm/ps, and a GVD coefficient of $|\beta_2| = 20$ ps^2/km. Then $l_N \sim 10$ cm. Although we have chosen a case of high power with large nonlinear coefficient as the example, ϵ is only 10^{-4}. ω_W and ω_D are ~ 2 ns^{-1} (320 MHz) and ~ 20 ps^{-1} (3.2 THz), respectively. Even for a large modulation frequency ~ 40 ps^{-1} (6.4 THz), ϵ_Ω is only $\sim 10^{-3}$.

By using the small-parameter analysis[16] in ϵ and ϵ_Ω, we obtain the following analytical expressions for the dispersion relations in Eq. (13):

$$k_{1\pm}(\omega) \approx \beta_1\omega \pm Y_1(\omega), \quad (14)$$

$$k_{2\pm}(\omega) \approx \beta_1\omega \pm Y_2(\omega), \qquad (15)$$

with

$$Y_1(\omega) = \sqrt{(\beta_2\omega^2/2 + \gamma|A_{10}|^2)^2 - (\gamma|A_{10}|^2)^2}, \quad (16)$$

$$Y_2(\omega) = \sqrt{(\beta_2\omega^2/2 + \gamma|A_{20}|^2)^2 - (\gamma|A_{20}|^2)^2}. \qquad (17)$$

The other coefficients in Eq. (13) are given by

$$r_{1+}(\omega) \approx (Y_1 - \beta_2\omega^2/2 - \gamma|A_{10}|^2)/(\gamma A_{10}^2), \qquad (18)$$

$$r_{1-}(\omega) \approx (Y_1 - \beta_2\omega^2/2 - \gamma|A_{10}|^2)/(\gamma A_{10}^{*2}), \qquad (19)$$

$$r_{2+}(\omega) \approx (Y_2 - \beta_2\omega^2/2 - \gamma|A_{20}|^2)/(\gamma A_{20}^2), \qquad (20)$$

$$r_{2-}(\omega) \approx (Y_2 - \beta_2\omega^2/2 - \gamma|A_{20}|^2)/(\gamma A_{20}^{*2}), \qquad (21)$$

$$e_{1++}(\omega) \approx -(Y_1 - \beta_2\omega^2/2)A_{20}/(\beta_1\omega A_{10}), \qquad (22)$$

$$e_{1+-}(\omega) \approx (Y_1 - \beta_2\omega^2/2)A_{20}^*/(\beta_1\omega A_{10}), \qquad (23)$$

$$e_{1-+}(\omega) \approx -(Y_1 - \beta_2\omega^2/2)A_{20}/(\beta_1\omega A_{10}^*), \qquad (24)$$

$$e_{1--}(\omega) \approx (Y_1 - \beta_2\omega^2/2)A_{20}^*/(\beta_1\omega A_{10}^*), \qquad (25)$$

$$e_{2++}(\omega) \approx -(Y_2 - \beta_2\omega^2/2)A_{10}/(\beta_1\omega A_{20}), \qquad (26)$$

$$e_{2+-}(\omega) \approx (Y_2 - \beta_2\omega^2/2)A_{10}^*/(\beta_1\omega A_{20}), \qquad (27)$$

$$e_{2-+}(\omega) \approx -(Y_2 - \beta_2\omega^2/2)A_{10}/(\beta_1\omega A_{20}^*), \qquad (28)$$

$$e_{2--}(\omega) \approx (Y_2 - \beta_2\omega^2/2)A_{10}^*(\beta_1\omega A_{20}^*). \qquad (29)$$

The procedure leading to the above expressions consists of solving Eqs. (9) and (10) for $\delta A_1(\omega, z)$ and $\delta A_1^*(-\omega, z)$ by first assuming $\delta A_2(\omega, z) = 0$ and $\delta A_2^*(-\omega, z) = 0$ and obtaining the dispersion relations $k_{1\pm}(\omega)$ and the coupling coefficients $r_{1\pm}(\omega)$. Next, we insert the obtained solutions for $\delta A_1(\omega, z)$ and $\delta A_1^*(-\omega, z)$ into Eqs. (11) and (12) to find $\delta A_2(\omega, z)$ and $\delta A_2^*(-\omega, z)$, which are related to the expressions for $e_{1\pm\pm}(\omega)$. The small parameters ϵ and ϵ_Ω have allowed us to use $Y_1 \ll \beta_1\omega$ and $\beta_2\omega^2 \ll \beta_1\omega$ to simplify expressions. Thus the dispersion relations and all the coupling coefficients for the c_1 and c_2 modes in Eq. (13) are obtained. The error introduced by this approximation is checked by putting the resulting $\delta A_2(\omega, z)$ and $\delta A_2^*(-\omega, z)$ (which, although very small, are nonzero) back into Eqs. (9) and (10) and verifying that the percentage error is relatively small. A similar procedure is used for the c_3 and c_4 modes in Eq. (13) by starting with Eqs. (11) and (12).

It can be shown from Eqs. (16)–(29) that the r's can be $O(1)$ while the e's are at most $O(\epsilon)$. The significance of this observation can be seen by referring to Eq. (13). For the c_1 and c_2 modes, the coupling between the two forward sidebands is represented by $r_{1\pm}(\omega)$ while the coupling to the two backward sidebands is represented by the $e_{1\pm\pm}(\omega)$'s. Comparing with the case of a single forward-pump wave, it is worth noticing that $r_{1\pm}(\omega)$ is not affected by the presence of the backward pump. Also, the dispersion relations $k_{1\pm}(\omega)$ for the c_1 and c_2 modes are the same as if the other pump wave did not exist. In the case of a single forward-pump wave, it is well known that the coupling between the the two forward sidebands is caused by FWM between the sidebands and the forward pump.[8] Thus the presence of a counterpropagating

pump wave introduces backward coupling into the eigenmodes through the coefficients $e_{1\pm\pm}$. The FWM picture of this coupling has been described in Ref. 8. Similar comments apply for the c_3 and c_4 modes with respect to the backward-pump wave.

C. Sideband Amplitudes

The above discussion indicates that the evolution of sidebands associated with the forward-pump wave, $\delta A_1(\omega, z)$ and $\delta A_1^*(-\omega, z)$, is affected only by the relatively weak additive contributions from the distributed feedback (DFB) occurring because of the presence of a backward-pump wave, and vice versa. However, when Y_1 and Y_2 become very small, the c_1 and c_2 modes (or c_3 and c_4 modes) become degenerate. This degeneracy suggests that Eq. (13) is not in a proper form to represent the general solution of Eqs. (9)–(12) in such a situation. Thus it is not clear what would be the magnitude of the backscattering contribution in general.

An answer is provided by the theory of Bragg gratings based on the coupled-mode equations.[8] Because of the DFB, each forward-propagating wave also has a contribution from the backward-propagating waves. To find a proper general solution that can include such a DFB, we transform the four constants c_1, c_2, c_3, and c_4 into c_{f+}, c_{f-}^*, c_{b+}, and c_{b-}^* by using the linear combinations

$$c_{f+} = c_1 + r_{1-}c_2, \quad c_{b+} = c_3 + r_{2-}c_4, \qquad (30)$$

$$c_{f-}^* = r_{1+}c_1 + c_2, \quad c_{b-}^* = r_{2+}c_3 + c_4. \qquad (31)$$

Physically, c_{f+} and c_{f-}^* represent the combinations of two forward-propagating sidebands, while c_{b+} and c_{b-}^* represent the combinations of two backward-propagating sidebands. The general solution given by Eq. (13) can be written in terms of the new constants as

$$\delta\mathbf{A}_1(\omega, z) = \exp(i\beta_1\omega z)\mathbf{M}_f(\omega, z)\mathbf{c}_f$$
$$+ \exp[i\beta_1\omega(l - z)]\mathbf{M}_{bf}(\omega, l - z)\mathbf{c}_b, \quad (32)$$

$$\delta\mathbf{A}_2(\omega, z) = \exp[i\beta_1\omega(l - z)]\mathbf{M}_b(\omega, l - z)\mathbf{c}_b$$
$$+ \exp(i\beta_1\omega z)\mathbf{M}_{fb}(\omega, z)\mathbf{c}_f, \qquad (33)$$

where $\mathbf{c}_f$ is the column vector formed by use of c_{f+} and c_{f-}^* as its two elements and $\mathbf{c}_b$ is another column vector formed by use of c_{b+} and c_{b-}^*. The vectors $\delta\mathbf{A}_1$ and $\delta\mathbf{A}_2$ are formed by use of the two forward and the two backward-propagating sidebands, respectively. The 2×2 matrices appearing in Eq. (32) are defined as

$$\mathbf{M}_f(\omega, z) = \frac{1}{1 - r_{1+}r_{1-}}\begin{bmatrix} 1 & r_{1-} \\ r_{1+} & 1 \end{bmatrix}$$
$$\times\begin{bmatrix} \exp(iY_1 z) & 0 \\ 0 & \exp(-iY_1 z) \end{bmatrix}$$
$$\times\begin{bmatrix} 1 & -r_{1-} \\ -r_{1+} & 1 \end{bmatrix}, \qquad (34)$$

$$\mathbf{M}_{fb}(\omega, z) = \frac{1}{1 - r_{2+}r_{2-}} \begin{bmatrix} e_{1++} & e_{1-+} \\ e_{1+-} & e_{1--} \end{bmatrix}$$

$$\times \begin{bmatrix} \exp(iY_1 z) & 0 \\ 0 & \exp(-iY_1 z) \end{bmatrix}$$

$$\times \begin{bmatrix} 1 & -r_{1-} \\ -r_{1+} & 1 \end{bmatrix}. \tag{35}$$

The matrix elements of $\mathbf{M}_f$ are found to be

$$M_{f11}(\omega, z) = [\exp(iY_1 z) - r_{1+}r_{1-}$$
$$\times \exp(-iY_1 z)]/(1 - r_{1+}r_{1-}), \tag{36}$$

$$M_{f12}(\omega, z) = r_{1-}[-\exp(iY_1 z)$$
$$+ \exp(-iY_1 z)]/(1 - r_{1+}r_{1-}), \tag{37}$$

$$M_{f21}(\omega, z) = r_{1+}[\exp(iY_1 z)$$
$$- \exp(-iY_1 z)]/(1 - r_{1+}r_{1-}), \tag{38}$$

$$M_{f22}(\omega, z) = (-r_{1+}r_{1-}\exp(iY_1 z)$$
$$+ \exp(-iY_1 z))/(1 - r_{1+}r_{1-}), \tag{39}$$

and the matrix elements of $\mathbf{M}_{fb}$ are

$$M_{fb11}(\omega, z) = [e_{1++}\exp(iY_1 z) - e_{1-+}r_{1+}$$
$$\times \exp(-iY_1 z)]/(1 - r_{1+}r_{1-}), \tag{40}$$

$$M_{fb12}(\omega, z) = [-e_{1++}r_{1-}\exp(iY_1 z) + e_{1-+}$$
$$\times \exp(-iY_1 z)]/(1 - r_{1+}r_{1-}), \tag{41}$$

$$M_{fb21}(\omega, z) = [e_{1+-}\exp(iY_1 z) - e_{1--}r_{1+}$$
$$\times \exp(-iY_1 z)]/(1 - r_{1+}r_{1-}), \tag{42}$$

$$M_{fb22}(\omega, z) = [-e_{1+-}r_{1-}\exp(iY_1 z) + e_{1--}$$
$$\times \exp(-iY_1 z)]/(1 - r_{1+}r_{1-}). \tag{43}$$

The expressions for $\mathbf{M}_b$ and $\mathbf{M}_{bf}$ are similar to $\mathbf{M}_f$ and $\mathbf{M}_{fb}$, respectively, because of the symmetry. Note $\mathbf{M}_f(\omega, 0) = \mathbf{1}$ and $\mathbf{M}_b(\omega, l) = \mathbf{1}$.

The two parts of the general solution, Eqs. (32) and (33), have a clear physical meaning. The forward- and backward-transfer matrices $\mathbf{M}_f$ and $\mathbf{M}_b$ give the transformation of the sidebands of the forward- and the backward-pump waves along their respective propagation distance as if the other pump wave did not exist, while the cross matrices $\mathbf{M}_{bf}$ and $\mathbf{M}_{fb}$ give the contribution to their evolution, from the other pump wave, that is due to backscattering (or DFB). Equations (32) and (33) are the main results of this section since they provide a simple model to describe evolution of the sidebands resulting from different physical mechanisms.

From Eqs. (34) and (35), it is easy to see that the relative magnitudes of $\mathbf{M}_{fb}$ and $\mathbf{M}_f$ are normally $O(\epsilon)$ unless the denominator $1 - r_{1+}r_{1-}$ is very small. A careful analysis shows that this would occur only when $|Y_1|/(\gamma|A_{10}|^2) \ll 1$, a condition equivalent to requiring either $\Omega \ll 1$ for both the normal and anomalous dispersion or $\Omega - 2 \ll 1$ for anomalous dispersion. Under these circumstances, the c_1 and c_2 modes are degenerate. However, because of our choice of the new set of con-

stants, Eqs. (32) and (33) remain a valid form of the general solution since the matrices elements are finite. In fact, it can be shown that when $\Omega \ll 1$, Eqs. (36)–(43) are reduced to

$$M_{f11} = 1 + i\gamma|A_{10}|^2 z, \tag{44}$$

$$M_{f12} = i\gamma A_{10}^2 z, \tag{45}$$

$$M_{f21} = -i\gamma A_{10}^{*2} z, \tag{46}$$

$$M_{f22} = 1 - i\gamma|A_{10}|^2 z, \tag{47}$$

$$M_{fb11} = -\gamma A_{10}^* A_{20}/(\beta_1 \omega), \tag{48}$$

$$M_{fb12} = -\gamma A_{10} A_{20}/(\beta_1 \omega), \tag{49}$$

$$M_{fb21} = \gamma A_{10}^* A_{20}^*/(\beta_1 \omega), \tag{50}$$

$$M_{fb22} = \gamma A_{10} A_{20}^*/(\beta_1 \omega). \tag{51}$$

Similar expressions hold for $\mathbf{M}_b$ and $\mathbf{M}_{bf}$. It turns out that these solutions exactly satisfy Eqs. (9)–(12) for $\beta_2 = 0$, which is not surprising because the condition $\Omega \ll 1$ implies that GVD is not important. Thus our general solutions, Eqs. (32) and (33), include the dispersionless case. This case has been studied previously,[1] and our results reduce to those obtained there. Equations (44)–(51) show that even in the degenerate case, the magnitude of the feedback matrix $\mathbf{M}_{fb}$ compared with that of the transfer matrix $\mathbf{M}_f$ is no more than $O(\epsilon/\Omega)$, and the same is true for $\mathbf{M}_{bf}$ and $\mathbf{M}_b$. This conclusion is quite general since it also holds when $\Omega \ll 1$ is not satisfied (including the case $\Omega - 2 \ll 1$ in the anomalous-dispersion regime).

The solution given by Eqs. (32) and (33) can also be written as

$$\begin{bmatrix} \delta\mathbf{A}_1(\omega, z) \\ \delta\mathbf{A}_2(\omega, z) \end{bmatrix} = \exp(i\beta_1 \omega z)\begin{bmatrix} \mathbf{M}_f(\omega, z) \\ \mathbf{M}_{fb}(\omega, z) \end{bmatrix}\mathbf{c}_f$$
$$+ \exp[i\beta_1 \omega(l - z)]$$
$$\times \begin{bmatrix} \mathbf{M}_{bf}(\omega, l - z) \\ \mathbf{M}_b(\omega, l - z) \end{bmatrix}\mathbf{c}_b. \tag{52}$$

The form of Eq. (52) shows that the general solution is the superposition of two modes represented by $\mathbf{c}_f$ and $\mathbf{c}_b$. In the case $\epsilon/\Omega \ll 1$ or $\omega \gg \omega_W$, the $\mathbf{c}_f$ mode is primarily forward propagating with weak backscattering, and the $\mathbf{c}_b$ mode is primarily backward propagating with weak forward scattering. In fact, Eq. (52) is the analog of a similar equation found in the theory of Bragg gratings[8] or DFB semiconductor lasers[17] in the limit of large detuning, except that M_j, M_{jk}, and c_j (j and $k = f$ or b) are scalar quantities in the later case. It is well known that in a largely detuned DFB structure, the c_f term describes the forward-propagation mode, with M_f and M_{fb} indicating the relative amplitudes of the forward-propagating and backscattered components, and a similar interpretation holds for the c_b term. Thus Eq. (52) is a generalized form that is appropriate when light at two different frequencies propagates through a Bragg grating. A large detuning is known to decrease the DFB. Similarly, a large walk-off effect for $\omega \ll \omega_W$ reduces the backscattering.

Equations (36)–(43) can be used to deduce several properties of the matrices $\mathbf{M}_f$ and $\mathbf{M}_{fb}$. In particular, note that $M_{f11}^*(-\omega, z) = M_{f22}(\omega, z)$, $M_{f12}^*(-\omega, z)$

$= M_{f21}(\omega, z), \qquad M_{fb11}^{*}(-\omega, z) = M_{fb22}(\omega, z), \qquad$ and $M_{fb12}^{*}(-\omega, z) = M_{fb21}(\omega, z)$, as required by the symmetry between ω and $-\omega$. Furthermore, it can be shown that $\mathbf{M}_{f}(-\omega, z) = \mathbf{M}_{f}(\omega, z)$ and $\mathbf{M}_{fb}(-\omega, z) = -\mathbf{M}_{fb}(\omega, z)$. Similar properties hold for $\mathbf{M}_{b}$ and $\mathbf{M}_{bf}$.

Examining the asymptotic behavior of $\mathbf{M}_{f}(\omega, z)$ over a distance l, we notice that besides oscillations, its magnitude can increase either linearly as l/l_{N} or exponentially as $\exp(l/l_{N})$. The latter case occurs in the anomalous-dispersion regime when $\Omega \sim (2)^{1/2}$ while the former happens whenever $|Y_{1}(\omega)|l \ll 1$, translating into the requirement of $\Omega \ll 1$ (i.e., nondispersive propagation) for both normal and anomalous regimes or $\Omega - 2 \ll 1$ for the anomalous regime. It is easy to see that the exponential growth is due to MI in the anomalous-dispersion regime. Similar properties hold for $\mathbf{M}_{b}$ in the backward direction. The amplification property of these transfer matrices is important because it leads to absolute instabilities when the system is subjected to external feedback. The next section considers the effect of boundary reflections that occur naturally in a FP cavity.

3. BOUNDARY REFLECTIONS

Before discussing the instabilities of counterpropagating pump waves in a dispersive Kerr medium, we generalize the analysis of Section 2 to include the feedback occurring at mirrors of a FP cavity. For simplicity, we assume that the two facets of the finite Kerr medium form the FP cavity (see Fig. 1) and write the boundary conditions at the front and rear surfaces of the Kerr medium as

$$\delta\mathbf{A}_{1}(\omega, 0) = \mathbf{R}_{f}\delta\mathbf{A}_{2}(\omega, 0), \qquad (53)$$

$$\delta\mathbf{A}_{2}(\omega, l) = \mathbf{R}_{b}\delta\mathbf{A}_{1}(\omega, l), \qquad (54)$$

where

$$\mathbf{R}_{f} = \begin{bmatrix} r_{f}\exp(i\psi_{rf}) & 0 \\ 0 & r_{f}\exp(-i\psi_{rf}) \end{bmatrix}, \qquad (55)$$

with a similar expression for $\mathbf{R}_{b}$ obtained by replacing the subscript f with b. Here, $\psi_{rf} = \phi_{rf} + \Delta_{2}$ and $\psi_{rb} = \phi_{rb} + \Delta_{1}$, where $\Delta_{1} = k_{0}l + \gamma(|A_{10}|^{2} + 2|A_{20}|^{2})l$ and $\Delta_{2} = k_{0}l + \gamma(|A_{20}|^{2} + 2|A_{10}|^{2})l$ are the linear and nonlinear phases associated with the propagation of the forward- and backward-pump waves, respectively. Further, $r_{f}\exp(i\phi_{rf})$ and $r_{b}\exp(i\phi_{rb})$ are the reflection coefficients for the front and rear boundaries.

By using Eqs. (32) and (33), we transform Eqs. (53) and (54) into

$$[\mathbf{1} - \mathbf{R}_{f}\mathbf{M}_{fb}(\omega, 0)]\mathbf{c}_{f} = \exp(i\beta_{1}\omega l)[\mathbf{R}_{f}\mathbf{M}_{b}(\omega, l)$$
$$- \mathbf{M}_{bf}(\omega, l)]\mathbf{c}_{b}, \qquad (56)$$

$$[\mathbf{1} - \mathbf{R}_{b}\mathbf{M}_{bf}(\omega, 0)]\mathbf{c}_{b} = \exp(i\beta_{1}\omega l)[\mathbf{R}_{b}\mathbf{M}_{f}(\omega, l)$$
$$- \mathbf{M}_{fb}(\omega, l)]\mathbf{c}_{f}. \qquad (57)$$

As a standard treatment, the solutions of Eqs. (56) and (57) in the complex-frequency domain ω represent an eigenvalue problem. In fact, similar equations can be found in the treatment of DFB lasers in the limit of large detuning, except that the vectors and matrices in the above are replaced by scalar quantities there. From a physical standpoint, the problem can be considered as a doubly resonant parametric oscillator[18] with the DFB included. The following algebraic equation for ω has to be satisfied for nontrivial solutions of $\mathbf{c}_{f}$ and $\mathbf{c}_{b}$:

$$D(\omega) = |\mathbf{1} - \exp(i2\beta_{1}\omega l)[\mathbf{R}_{f}\mathbf{M}_{b}(\omega, l) - \mathbf{M}_{bf}(\omega, l)]$$
$$\times [\mathbf{1} - \mathbf{R}_{b}\mathbf{M}_{bf}(\omega, 0)]^{-1}[\mathbf{R}_{b}\mathbf{M}_{f}(\omega, l)$$
$$- \mathbf{M}_{fb}(\omega, l)] \times [\mathbf{1} - \mathbf{R}_{f}\mathbf{M}_{fb}(\omega, 0)]^{-1}| = 0. \qquad (58)$$

The multiple solutions ω_{n} (n is an integer) of Eq. (58) stand for different longitudinal "supermodes" of the system. The real part of each solution gives the mode position and the imaginary part gives the growth or damping rate. Absolute instability occurs whenever ω_{n} has a positive imaginary part. By substituting $\mathbf{c}_{fn}$ and $\mathbf{c}_{bn}$, obtained by substituting Eqs. (56) and (57) into Eq. (52), we can calculate the eigenfields corresponding to each supermode. It is evident that there are generally two counterpropagating pairs of sidebands for each longitudinal mode. Therefore the eigenfields correspond to pulsing in the spatiotemporal domain.

Equation (58) can be simplified by dividing the parameter space into several regions. From the discussion in Section 2, we know that if $\Omega \ll 1$, this equation will reduce to the dispersionless case, which has been studied before.[1] Therefore we assume $\Omega \gg \epsilon$ so that the magnitudes of $\mathbf{M}_{fb}(\omega, 0)$ and $\mathbf{M}_{bf}(\omega, 0)$ are much less than unity. Then the two inverse matrices in Eq. (58) can be approximated by unity, and we obtain

$$D(\omega) = |\mathbf{1} - \exp(i2\beta_{1}\omega l)[\mathbf{R}_{f}\mathbf{M}_{b}(\omega, l) - \mathbf{M}_{bf}(\omega, l)]$$
$$\times [\mathbf{R}_{b}\mathbf{M}_{f}(\omega, l) - \mathbf{M}_{fb}(\omega, l)]| = 0. \qquad (59)$$

For very small ϵ, there can be a region, $1 \gg \Omega \gg \epsilon$, overlapped by the cases considered in this paper and in Ref. 1. In this region, the frequency is low enough that dispersion is not important, yet high enough that cross coupling or DFB is weak.

4. WEAK BOUNDARY REFLECTIONS

The solutions of Eq. (59) can be divided into two categories. If the magnitudes of boundary-reflection coefficients are much larger than $O(\epsilon/\Omega)$, the cross-matrix terms in Eq. (59) are much smaller than the transfer-matrix terms and can therefore be neglected. Physically, the localized feedback at the facets is much stronger than the weak DFB, and the latter effect can be ignored. Since ϵ is quite small, even relatively weak reflections such as those occurring at the uncoated air–glass boundary (power reflectivity of ~4%) fit into this category. This case is discussed in part II (the accompanying paper

in this issue[19]). Here, we discuss the case occurring when the boundary-reflection coefficients are comparable to or less than $O(\epsilon/\Omega)$. This case may occur in practice even when antireflection coatings are used to suppress facet reflections.

In the case of weak reflections, Eq. (59) can be further simplified by using the relation

$$|1 - \exp(i2\beta_1\omega l)\mathbf{U}| = 1 - \exp(i2\beta_1\omega l)\text{Tr}\mathbf{U}$$
$$+ \exp(i4\beta_1\omega l)|\mathbf{U}|, \qquad (60)$$

where the 2×2 matrix $\mathbf{U}$ is defined as

$$\mathbf{U} = [\mathbf{R}_f\mathbf{M}_b(\omega, l) - \mathbf{M}_{bf}(\omega, l)][\mathbf{R}_b\mathbf{M}_f(\omega, l)$$
$$- \mathbf{M}_{fb}(\omega, l)]. \qquad (61)$$

It is useful to introduce a scalar quantity $g(\omega) = \text{Tr }\mathbf{U}$ and write Eq. (59) as

$$D(\omega) = 1 - \exp(i2\beta_1\omega l)g(\omega) = 0, \qquad (62)$$

where

$$g(\omega) = (R_{f11}M_{b11} - M_{bf11})(R_{b11}M_{f11} - M_{fb11})$$
$$+ (R_{f11}M_{b12} - M_{bf12})(R_{b11}^*M_{f12}^* + M_{fb12}^*)$$
$$+ (R_{f11}^*M_{b12}^* + M_{bf12}^*)(R_{b11}M_{f12} - M_{fb12})$$
$$+ (R_{f11}^*M_{b11}^* + M_{bf11}^*)(R_{b11}^*M_{f11}^* + M_{fb11}^*).$$
$$(63)$$

For consistency, we have neglected $|\mathbf{U}|$ since, by using Eqs. (34) and (35), we conclude that its amplitude is independent of l and is at most $O(\epsilon/\Omega)^4$ (for $|r_f|, |r_b| \approx \epsilon$), which is much smaller than unity. Actually, one can prove that $|\mathbf{U}|$ can be neglected as long as $|r_f|, |r_b| \ll 1$. Equation (62) is in a standard form for the laser threshold condition with $g(\omega)$ representing the net gain. Thus $|g(\omega)| > 1$ is required for an absolute instability to occur.

From Eq. (63), it is evident that for the case of weak boundary reflections ($|r_f|, |r_b| \sim \epsilon$) under consideration, $|g|$ is at most $O(\epsilon/\Omega)^2$ when the normalized length $L = l/l_N \lesssim 1$, and the system is below instability threshold. As L increases, $|g|$ can increase either as L^2 (for both the normal- and anomalous-dispersion regimes) or as $\exp(2L)$ in the anomalous-dispersion regime when $\Omega \sim (2)^{1/2}$. For the case of quadratic amplification that occurs when GVD is negligible, previous results[1] indicate

that the threshold condition requires L to be $O[1/(|r_fr_b|)^{1/2}]$. This represents a very high threshold in the case of weak boundary reflections. On the other

hand, the exponential amplification in the anomalous region requires L to be $O[\ln(\Omega/\epsilon)]$ to reach threshold, a condition much easier to satisfy. For this reason, we concentrate on the anomalous-dispersion case with $\Omega \approx O(1)$. By use of Eqs. (36)–(43), Eq. (63) becomes

$$g(\omega) = \{\exp(-iY_2l)[r_1e_2 + e_2 + r_1r_2r_f \exp(i\theta_f)$$
$$- r_f \exp(-i\theta_f)][r_2e_1 + e_1 + r_2r_1r_b \exp(i\theta_b)$$
$$- r_b \exp(-i\theta_b)] - \exp(iY_2l)[r_1e_2 + e_2$$
$$+ r_1r_f \exp(i\theta_f) - r_2r_f \exp(-i\theta_f)][r_2e_1 + e_1$$
$$+ r_1r_b \exp(i\theta_b) - r_2r_b \exp(-i\theta_b)]\}$$
$$\times \exp(-iY_1l)/[(1 - r_1^2)(1 - r_2^2)], \qquad (64)$$

with

$$r_1(\omega) = (Y_1 - \beta_2\omega^2/2)/(\gamma|A_{10}|^2) - 1, \qquad (65)$$

$$r_2(\omega) = (Y_2 - \beta_2\omega^2/2)/(\gamma|A_{20}|^2) - 1, \qquad (66)$$

$$e_1(\omega) = (r_1 + 1)\gamma|A_{10}A_{20}|/(\beta_1\omega), \qquad (67)$$

$$e_2(\omega) = (r_2 + 1)\gamma|A_{10}A_{20}|/(\beta_1\omega), \qquad (68)$$

$$\theta_f = \phi_{rf} + k_0l + \gamma(|A_{20}|^2 + 2|A_{10}|^2)l$$
$$+ \phi_{20} - \phi_{10}, \qquad (69)$$

$$\theta_b = \phi_{rb} + k_0l + \gamma(|A_{10}|^2 + 2|A_{20}|^2)l$$
$$+ \phi_{10} - \phi_{20}, \qquad (70)$$

where we have ignored $\exp(-|Y_1|l)$ compared with $\exp(|Y_1|l)$ since $\exp(|Y_1|l) \approx \Omega/\epsilon$ for reaching the MI threshold. However, $\pm iY_2(\omega)$ can be imaginary within the MI frequency range of the forward pump since we have assumed that the ratio S of the backward- and forward-pump powers satisfies $S = |A_{20}|^2/|A_{10}|^2 \leqslant 1$.

Equation (64) can be further simplified when the boundary reflections can be completely ignored for $|r_f|, |r_b| \ll \epsilon$. The instability gain is then given by

$$g(\omega) = -i\frac{\gamma^2|A_{10}|^2|A_{20}|^2\beta_2^2\omega^2}{2\beta_1^2Y_1Y_2} \exp(-iY_1l)\sin(Y_2l).$$
$$(71)$$

In terms of the normalized frequency Ω and the normalized length L, $g(\omega)$ becomes

$$g(\omega) = \epsilon^2\bar{g}(\Omega, L), \qquad (72)$$

where

$$\bar{g}(\Omega, L) = -\frac{S\Omega^2 \exp[L\sqrt{1 - (\Omega^2/2 - 1)^2}] \sin[L\sqrt{(\Omega^2/2 - S)^2 - S^2}]}{2\sqrt{1 - (\Omega^2/2 - 1)^2}\sqrt{(\Omega^2/2 - S)^2 - S^2}}. \qquad (73)$$

Equation (62) can then be written as

$$1 - \epsilon^2 \exp(i2\Omega L/\epsilon)\bar{g}(\Omega, L) = 0. \qquad (74)$$

Equation (74), which is still in a standard form to describe the threshold of DFB lasers, can be easily analyzed since ϵ is a small parameter. Different values of Ω for which Eq. (74) is satisfied correspond to the various longitudinal supermodes mentioned earlier. First, we note that the mode spacing is only $\sim \epsilon/L$, while the gain $\bar{g}(\Omega, L)$ varies on the frequency scale of $1/L$. Thus various modes can be considered continuously distributed under the gain curve. Then, for any mode frequency Ω_r, the growth (or damping) rate is a small quantity given by

$$\Omega_i = \epsilon \ln[\epsilon^2|\bar{g}(\Omega_r, L)|]/(2L). \tag{75}$$

When written in terms of the physical units, the growth rate becomes

$$\omega_i = \ln|g(\omega_r)|/(2l\beta_1). \tag{76}$$

When compared with the previous numerical work,[4] Eqs. (71)–(76) not only give analytic results that are valid for arbitrary power ratios, but also provide a simple physical characterization of the instability in terms of the familiar language of laser oscillation. By using Eq. (75), Fig. 2(a) shows, as a numerical example, the MI growth rate as a function of the perturbation frequency for two different lengths of the Kerr medium corresponding to $L = 9$ (dashed curve) and $L = 12$ (solid curve) assuming equal pump powers ($S = 1$). Figure 2(b) is obtained under the identical conditions except that the power ratio $S = 0.5$. The oscillatory behavior in Fig. 2(b) occurs when Y_2 is real in the frequency region where the less intense backward-pump wave is modulationally stable. In such a region, the nonlinear phase shift $Y_2(\omega)l$ can cause constructive or destructive interference.
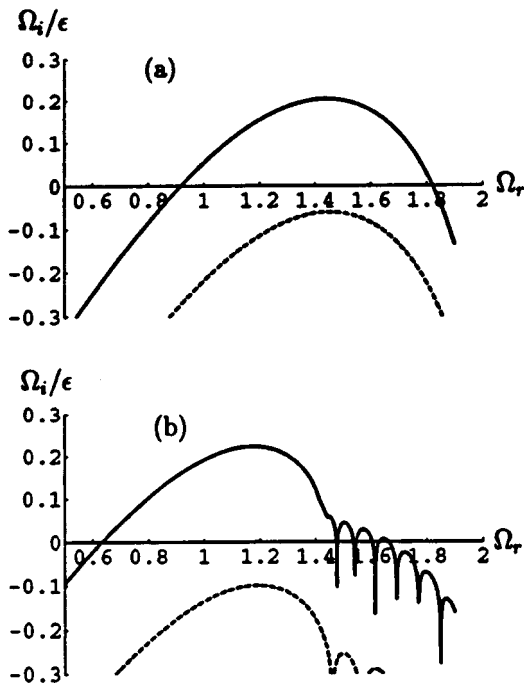
Fig. 2. Normalized growth rate Ω_i/ϵ of the absolute instability plotted as a function of normalized frequency Ω_r for $\epsilon = 1 \times 10^{-4}$. (a) $S = 1$ (equal pump powers) with $L = 9$ (dashed curve) and $L = 12$ (solid curve). (b) $S = 0.5$ (unequal pump powers) with $L = 12$ (dashed curve) and $L = 20$ (solid curve).
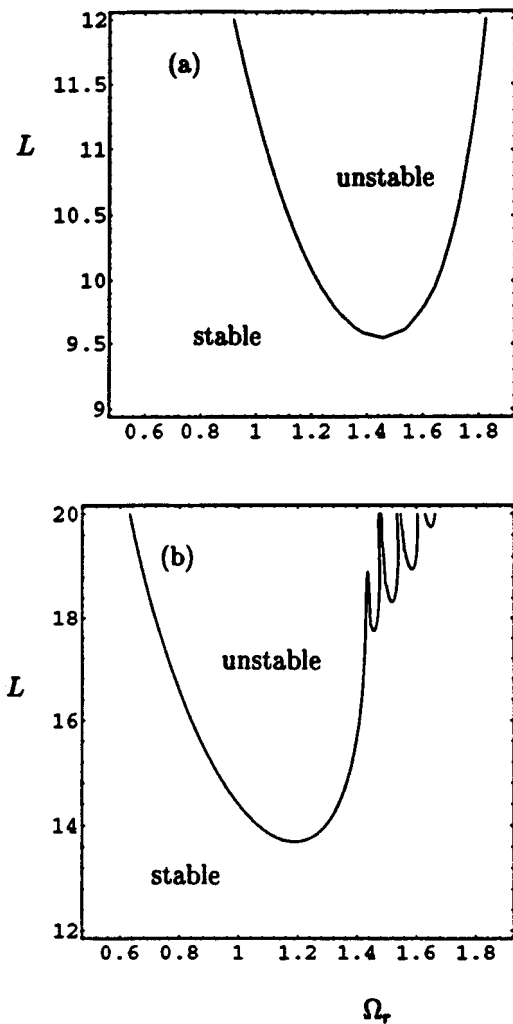
Fig. 3. Threshold condition for absolute instability to occur plotted in the Ω_r–L plane by use of $\epsilon = 1 \times 10^{-4}$ for (a) $S = 1$ and (b) $S = 0.5$.

The threshold condition for the onset of the absolute instability is obtained by finding the parameters for which the instability growth rate first becomes positive, i.e., by setting the right side of Eq. (75) or Eq. (76) to zero. Thus the threshold condition is just given by $|\epsilon^2\bar{g}(\Omega_r, L)| = 1$. Figures 3(a) and 3(b) show the threshold curves for two different power ratios by use of Eq. (73). In each case, the area above the curve indicates the instability region. Oscillation in Fig. 3(b) is caused by similar conditions as for Fig. 2(b).

For an order-of-magnitude estimate of the instability threshold, let us assume equal pump powers. This case has been numerically investigated previously[4] and allows a comparison with the previous work. Setting $S = 1$, the threshold condition can be written as

$$L = \frac{\ln(4 - \Omega^2) - 2\ln\epsilon}{\Omega(4 - \Omega^2)^{1/2}}, \tag{77}$$

where we have used $\sin\{L[(\Omega^2/2 - S) - S^2]^{1/2}\} \approx i\exp\{L[S^2 - (\Omega^2/2 - S)^2]^{1/2}\}/2$ in Eq. (73). From Eq.

(77), the minimum L, or the threshold of the instability, occurs at $\Omega = (2)^{1/2}$, which is the frequency for the maximum MI gain at a given pump power. In general, L is approximately $-\ln(\epsilon)$. This is in agreement with the previous work.[4,5] For the numerical values of $\epsilon \approx 10^{-4}$ used in Figs. 2 and 3, $L \approx 9$ corresponding to a physical length of the Kerr medium of $l \approx 1$ m. In the normalized units, the mode spacing is $\sim \epsilon \Omega_D / L$. In frequency units, mode spacing becomes 0.2×10^9 rad/s or ~ 30 MHz for our example. The growth rate is of the same order of magnitude as the mode spacing as seen from Eq. (75).

Although the above conclusions [including Eq. (76)] were drawn under the special case of negligible boundary reflections, they are valid in general since a similar analysis can be applied even when boundary reflections are included. The only difference is that we have to use Eq. (64) instead of Eq. (71) to include the effects of weak boundary reflections. Figure 4(a) shows the effects of boundary reflections on the growth rate under conditions identical to those of Fig. 2(a) except that both facets of the dispersive Kerr medium are assumed to have an amplitude-reflection coefficient of 5×10^{-4}. Figure 4(b) shows changes in the threshold curve and should be compared with Fig. 3(a). It is evident from Fig. 4 that a
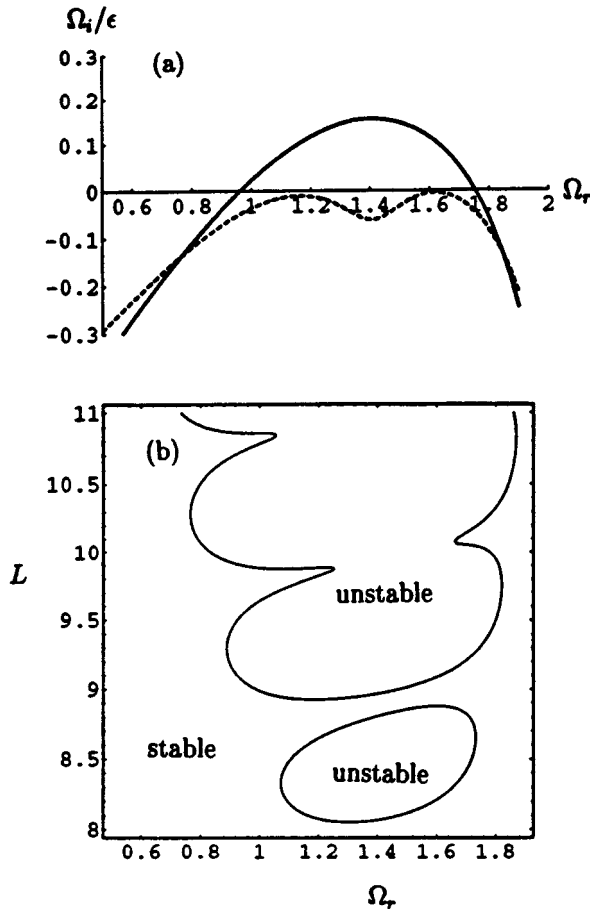
Fig. 4. Effects of weak boundary reflections on the absolute instability shown in Figs. 2 and 3 for $\epsilon = 1 \times 10^{-4}$, $r_f = r_b = 5 \times 10^{-4}$, and $S = 1$. (a) Ω_i / ϵ versus frequency Ω_r for $L = 9$, $\theta_f = \theta_b = \pi/2$ (dashed curve), and $\theta_f = \theta_b = 0$ (solid curve). (b) Threshold curves in the Ω_r–L plane, for $\phi_{rf} = \phi_{rb} = k_0 l = 0$ and $\phi_{20} = \phi_{10}$.

power reflectivity as small as 2.5×10^{-7} produces significant changes in the instability domain, indicating that one must include the effects of residual reflectivity even when antireflection coatings or isolators are used experimentally to reduce the effects of feedback.

The reason why even weak boundary reflections can substantially affect both the instability region and the growth rate of the instability can be understood by noting that the parameter ϵ is quite small under typical experimental conditions. If the amplitude reflection coefficients of the two facets are comparable to ϵ (which is $\sim 10^{-4}$ in the example used here), the DFB and the facet feedback can become in phase or out of phase with respect to each other, depending on the modulation frequency. Such interference effects are responsible for the drastic changes occurring with weak boundary reflections. Unlike the Ikeda instability, which vanishes when the feedback becomes negligible, the above instability exists and cannot be avoided by use of antireflection coatings on the boundaries. While Ikeda instability draws on the linear or quadratic spatial growth of dispersionless FWM, the absolute instability discussed here results from the exponential spatial growth of MI occurring in the anomalous-GVD regime. The normal-dispersion case with relatively strong boundary reflections is discussed in part II.[19]

The treatment in this section is valid as long as the boundary reflection coefficients are much smaller than one. The case of strong boundary reflections with amplitude-reflection coefficients much larger than ϵ is treated in part II.[19] Most experiments with fibers are likely to fall under the category of strong reflections, and the results of part II are more realistic for them. However, the results of this section can be important when applied to materials with a relatively large ϵ (but still much smaller than unity).

5. CONCLUSIONS

In this paper, the interaction of cw counterpropagating pump waves in a finite-size dispersive Kerr medium has been analytically studied. We have shown that, for small modulation frequencies such that the walk-off length is less than or comparable to the nonlinear length, the system can be considered dispersionless since the dispersion length is normally much longer than the nonlinear length in such cases.

To study the effect of GVD, we concentrated on the case when this condition is not satisfied and find that the coupling between the two counterpropagating pairs of sidebands is very weak. This is because when dispersion is important (i.e., when the dispersion length is comparable to the nonlinear length), the walk-off length is so short that the counterpropagating sidebands cannot interact over a long duration. Consequently, the evolution of each pair of sidebands is mostly determined by the corresponding pump wave alone, which provides a coupling between its two sidebands through the combined action of self-phase modulation and GVD. The effect of the counterpropagating pump wave is to provide a weak back-

scattering (or DFB) induced by cross-phase modulation to the propagation of two sidebands.   Based on this physical insight, we have developed a model that turns out to be a generalization of the treatment of DFB lasers with a large detuning.   The model also applies to the interaction of two beams in a doubly resonant parametric oscillator.[18]

In this first of a series of two papers we have focused on the case in which weak boundary reflections are as important as the DFB.   We find that for absolute instabilities to occur, the anomalous dispersion is needed to provide sufficient gain from MI.   Each longitudinal supermode of the absolute instability consists of two counterpropagating pairs of sidebands, corresponding to self pulsing in the output.   Analytical results for both the growth rate and the threshold conditions for the instability are obtained easily from the simple physical model constructed.   In the special case of equally intense counterpropagating pump beams and no boundary reflections, our results are in complete agreement with previous numerical work.

ACKNOWLEDGMENTS

REFERENCES

1. W. J. Firth, Opt. Commun. **39**, 343 (1981).
2. Y. Silberberg and I. Bar-Joseph, J. Opt. Soc. Am. B **1**, 662 (1984).
3. W. J. Firth and C. Paré, Opt. Lett. **13**, 1096 (1989); W. J. Firth, C. Paré, and A. FitzGerald, J. Opt. Soc. Am. B **7**, 1087 (1990).
4. C. T. Law and A. E. Kaplan, Opt. Lett. **14**, 734 (1989); J. Opt. Soc. Am. B **8**, 58 (1991).
5. W. J. Firth and C. Penman, Opt. Commun. **94**, 183 (1992).
6. R. W. Boyd, *Nonlinear Optics* (Academic, Boston, 1992).
7. K. Ikeda, Opt. Commun. **30**, 257 (1979).
8. G. P. Agrawal, *Nonlinear Fiber Optics*, 2nd ed. (Academic, San Diego, Calif., 1995).
9. R. Vallée, Opt. Commun. **81**, 419 (1991); Opt. Commun. **93**, 389 (1992).
10. M. B. van der Mark, J. M. Schins, and A. Lagendijk, Opt. Commun. **98**, 120 (1993).
11. G. Steinmeyer, D. Jaspert, and F. Mitschke, Opt. Commun. **104**, 379 (1994).
12. M. Nakazawa, K. Suzuki, and H. A. Haus, IEEE J. Quantum Electron. **25**, 2036 (1989); M. Nakazawa, K. Suzuki, H. Kubota, and H. A. Haus, IEEE J. Quantum Electron. **25**, 2045 (1989).
13. M. Haelterman, S. Trillo, and S. Wabnitz, Opt. Commun. **91**, 401 (1992); Opt. Lett. **17**, 745 (1992).
14. D. W. McLaughlin, J. V. Moloney, and A. C. Newell, Phys. Rev. Lett. **54**, 681 (1985).
15. M. Haelterman, Opt. Lett. **17**, 792 (1992).
16. A. H. Nayfeh, *Introduction to Perturbation Techniques* (Wiley, New York, 1981).
17. G. P. Agrawal and N. K. Dutta, *Semiconductor Lasers*, 2nd ed. (Van Nostrand Reinhold, New York, 1993), Chap. 7.
18. Y. R. Shen, *The Principles of Nonlinear Optics* (Wiley, New York, 1984), Chap. 9.
19. Y. Yu, C. McKinstrie, and G. P. Agrawal, J. Opt. Soc. Am. B **14**, 617 (1998).